Article

Field Measurements of Building Air-Conditioning Heat Rejection and the Thermal Environment in Urban Areas

Kang Mu *[ORCID], **Qiong Suo, Fangliang Ding, Changwei Jiang, Xiaofeng Zhang and Jing Ye**

College of Energy and Power Engineering, Changsha University of Science & Technology, Changsha 410114, China; suoq@stu.csust.edu.cn (Q.S.); 23206041396@stu.csust.edu.cn (F.D.); jiangcw@csust.edu.cn (C.J.); xiaofengzhang@csust.edu.cn (X.Z.); 22206041333@stu.csust.edu.cn (J.Y.)
* Correspondence: mukang@csust.edu.cn; Tel.: +86-18874970451

Abstract: In recent years, the surge in air-conditioning ownership and usage has led to significant heat rejection, impacting the surrounding atmosphere. Despite this, studies examining the spatiotemporal effects of air-conditioning heat rejection at a block scale remain limited. Additionally, comparative studies on the role of building areas with air-conditioning systems versus natural underlying surfaces in the urban thermal environment are relatively scarce. This study employs field measurements and ArcGIS technology to investigate the local thermal and humidity environments, as well as the spatiotemporal distribution of heat rejection from air-conditioning systems in Wuyi Square, Changsha. Results show that cooling tower exhausts in commercial buildings maintain relative humidity levels of 95.2% to 99.8% during the day, enhancing surrounding humidity. At night, the humidity aligns with atmospheric levels (from 50.3% to 62.5%). The cooling tower exhaust temperature is approximately 2.2 °C lower during the day and 2.4 °C higher at night compared to the surrounding temperatures. In contrast, exhausts from split-type air-conditioning units in residential buildings have an average relative humidity about 14.2% lower than the atmosphere humidity, with temperature averages being 5.2 °C higher during the day and 6.5 °C higher at night, raising surrounding temperatures. The study also finds that natural surface areas are up to 3.1 °C cooler and 9.6% more humid compared to built environment surfaces. Furthermore, residential areas have air temperatures about 0.3 °C higher than commercial zones, with a humidity distribution approximately 0.5% lower. These findings offer a theoretical foundation for enhancing urban thermal environments and informing urban planning and design.

Keywords: air-conditioning heat rejection; thermal environment; mobile measurement; underlying surface

1. Introduction

In recent years, urbanization has accelerated, becoming an inevitable trend in the context of global economic integration. Accompanying this expansion in urban areas, the surge in population has also had a significant impact on global climate change. Urban thermal climate issues like urban heat islands (UHI), urban wet islands, and global warming have become more prominent. The urban thermal climate impacts human health, comfort, and energy consumption [1]. City blocks are fundamental units in urban planning and design. The thermal environment of these blocks directly influences pedestrian comfort and health. Thus, in-depth research on the thermal environment of city blocks is essential for creating green, sustainable cities. Urban thermal climate is a complex phenomenon influenced by factors such as underlying surface types, heat-absorbing materials, and

anthropogenic heat emissions [2,3]. Areas with abundant vegetation and water can cool their surroundings locally [2]. Indeed, the release of anthropogenic heat from buildings, particularly through heat rejection from air conditioning and other heating systems, is considered a major contributor to the urban heat climate. It is estimated that this building-related heat release accounts for approximately 50% to 65% of the total anthropogenic heat in cities [4,5]. Notably, air-conditioning systems constitute a significant portion of China's building energy consumption, accounting for approximately 60% of total energy use in buildings [6]. Furthermore, the proportion of anthropogenic heat from building air-conditioning systems is steadily increasing. In China, the adoption rate of air conditioning is expected to increase from 82.5% to 95% between 2017 and 2090 [7]. Heat rejection from air-conditioning systems is directly emitted into neighborhoods, exacerbating the UHI effect. The UHI effect significantly increases energy demand for air conditioning in urban buildings [8], creating a vicious cycle. Therefore, there exists a strong correlation between the heat rejection from building air-conditioning systems and the urban thermal climate. These systems, while maintaining indoor thermal conditions, primarily influence the neighborhood's thermal environment and pedestrian comfort through temperature and humidity changes. To mitigate the urban heat climate and support sustainable economic growth, it is crucial to investigate how exhaust air temperature and humidity from air-conditioning systems affect the surrounding thermal conditions. This research is highly relevant to urban planning and environmental management.

Currently, research on the impact of heat rejection from building air-conditioning systems on the urban thermal climate is largely focused on the large-scale urban level. Hsieh et al. [9] used Energy Plus and CFD simulations to investigate the temporal variation and spatial distribution of temperature in the urban canopy. Their study specifically examined the influence of heat rejection from air-conditioning systems. The results indicated that temperatures increase with height, and the temperatures near buildings are consistently higher than those at atmospheric levels. Sun et al. [10] found that the cooling energy consumption of buildings influenced by the heat island effect correlates with city size. Liu et al. [11] examined indoor electricity consumption for heating and its effects on the outdoor thermal environment. Their results indicated that daytime air-conditioning operation had no significant impact on near-surface air temperature; however, nighttime temperatures increased by approximately 0.6 °C. Despite significant progress in studying heat rejection from building air-conditioning systems, detailed research on the effects of various forms of heat rejection on urban thermal climates remains limited, both domestically and internationally.

Methods for studying urban thermal climates include ground-based observations, remote sensing, and numerical modeling [12,13]. Wetherley et al. [14] analyzed urban energy flux variability across land cover and climate gradients in Los Angeles County, USA. They utilized high-resolution remote sensing along with spatial distribution simulations from an urban energy balance model. Meng et al. [15] used remote sensing to study UHI effects on cooling and heating energy demands of residential buildings in three cities of varying sizes in the Beijing–Tianjin–Hebei region. Findings indicate that as UHI intensity increases, the thermal load disparity between urban and rural areas decreases. Notably, the difference in cooling energy demands indicates that the hourly absolute load variation during the heating season is significantly greater than during the cooling season. This variation features higher nighttime loads and lower daytime loads in the heating season. Tariku et al. [16] used numerical simulations to predict urban canopy layer temperatures and building energy demands in Vancouver's central business district. Their findings revealed that the UHI effect leads to a 23% increase in the total cooling energy requirements and a 29% decrease in the total heating energy consumption of buildings. This results

in a negative overall impact on the comprehensive energy needs of the building stock. Zhong et al. [17] studied the impact of heat rejection from hybrid-mode outdoor units on the surrounding environment and the building cooling load by, coupling Energy Plus with Fluent. Their results indicate that the hybrid operation mode significantly reduces the negative impact of heat rejection on space cooling energy consumption compared to the all-air-conditioning operation. Increasing the outdoor unit's air supply rate leads to a slight increase in space cooling demand. However, these methods are typically applied in large-scale studies, and satellite remote sensing is sensitive to atmospheric conditions. The accuracy and reliability of numerical modeling techniques require further validation through actual measurements. Therefore, comprehensive field measurements of the thermal environment of city blocks are essential to fully understand the impact of air conditioning system heat rejection on the block scale.

This paper focuses on the impact of building air-conditioning heat rejection on urban heat climate, specifically in the Wuyi Square area of Tianxin District, Changsha City. Using field measurement methods, the study thoroughly investigates the effects of heat rejection from air conditioning systems on the atmosphere. The study also integrates GIS spatial analysis to visualize the thermal and humidity parameters of the neighborhood's surface environment. It explores the temporal distribution differences in thermal and humidity parameters across various building types and natural surfaces affected by air-conditioning heat rejection. This research aims to provide guidance for optimizing parameters to enhance the thermal environment of urban neighborhoods.

2. Methods

2.1. Details of the Studied Area

This study focused on Wuyi Square in the Tianxin District of Changsha, Hunan Province as a case study for the summer heat and humidity parameters (see Figure 1). Continuous measurements were taken to evaluate the heat rejection characteristics of air-conditioning systems and to perform mobile assessments of the thermal and humidity environment.

Figure 1. Study area. Case 1 denotes commercial buildings; case 2 denotes residential buildings.

2.2. Air-Conditioning Heat Exhaust Measurements

2.2.1. Measurements Area

This study selected the Changsha IFS Commercial Center, located at the core of Wuyi Square, as an example of a commercial building for the heat rejection measurements (see Case 1 in Figure 1). The area covers approximately 160,128 m^2, with a building density of

73%. This location experiences substantial atmospheric heat rejection from air-conditioning systems throughout the day, significantly affecting the urban thermal and humidity climate.

Additionally, a residential community on Dengren Street was selected to assess the heat rejection in residential buildings (see Case 2 in Figure 1). This area spans approximately 13,500 m^2, with a floor area ratio of 3.6, a greening rate of 43%, and a building density of 27.4%.

To analyze the impact of air-conditioning heat rejection from various building types and the underlying surface on the urban thermal and humidity environments of the urban blocks, the study area was divided into 10 sub-regions based on the layout of the main streets. As shown in Figure 2, Zones 1 to 10 represent these sub-regions. Specifically, Zones 1, 3, 5, 6, 7, and 8 mainly consisted of residential buildings, while Zones 2 and 4 were primarily commercial. Zone 10 featured water as the primary underlying surface, while Zone 9 included vegetation along with some residential buildings.
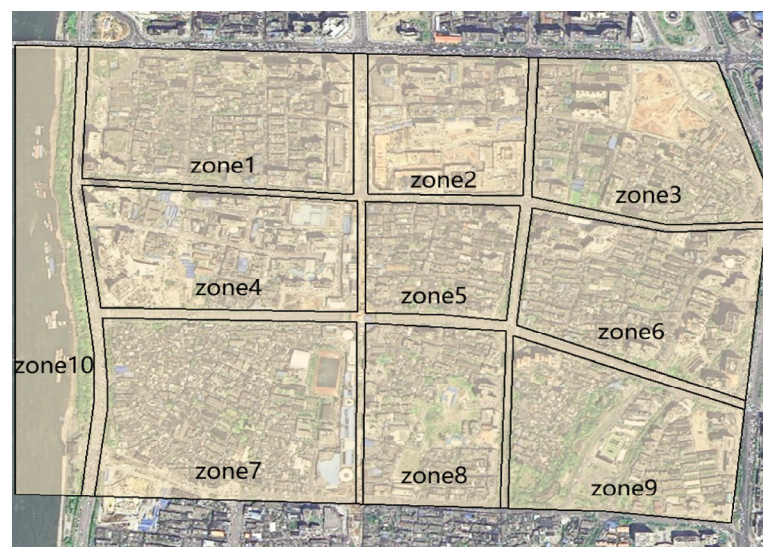

Figure 2. Regional distribution. Zones 1 to 10 represent these sub-regions.

2.2.2. Measurement Parameters and Methods

To investigate the heat rejection patterns of air-conditioning systems and their impact on the atmospheric thermal and humidity environment, the following key parameters were measured, temperature and relative humidity. In commercial buildings, cooling towers served as the primary heat rejection equipment, while residential buildings utilized split air-conditioning outdoor units. Figure 3 shows the measurement points for air-conditioning heat rejection. The study was conducted with a continuous measurement period spanning from 9 August to 15 August, targeting the week with the highest energy consumption and heat rejection. COS-04-X (Shandong Renke Measurement and Control Technology Company Ltd., Jinan, China) outdoor temperature and humidity data loggers were installed at the heat rejection devices for both systems, with an additional logger for atmospheric temperature at a weather station located in an open, non-built-up area. To minimize solar radiation interference, radiation shields were fitted on each instrument.

Figure 3. The measurement for air-conditioning heat rejection. The upper part of the picture shows the cooling tower measurement points, and the lower part of the picture shows the air-conditioning outdoor unit measurement points.

2.3. Mobile Measurement

Mobile measurements were widely used in the study of the local urban climates [18]. To obtain comprehensive and accurate data on the thermal and humid parameters of urban blocks, this research conducted mobile measurements in the case study area. This approach aimed to visually demonstrate the impact of heat rejection from air-conditioning systems in commercial and residential buildings on the surrounding thermal and humid environment, while also providing raw data for ArcGIS 10.6 analysis.

2.3.1. Mobile Route

To obtain continuous spatiotemporal data on the thermal and humidity parameters in urban neighborhoods and to visualize the impact of heat rejection from air-conditioning systems, this study aimed to cover a variety of building types and underlying surfaces. Fixed weather stations were established within the study area to calibrate temporal and spatial data. Figure 4 illustrates the mobile routes and the locations of the fixed weather stations, numbered 1 to 4. Weather Station 1 was situated within a commercial building complex that primarily utilized cooling towers for heat rejection. Weather Station 2 was located in a residential complex where split-type air conditioners served as the main heat rejection source. Weather Station 3 was placed by the river, where water served as the underlying surface, while Weather Station 4 was located in a park with vegetation as the underlying surface. The mobile route covered a total length of 6.5 km.

Figure 4. Mobile route and fixed weather station locations. The four numbers denote the locations of the fixed weather stations placed in different regions. The red line denotes the track of the move.

2.3.2. Mobile Testing Scheme

This study selected four typical daytime moments (10:00, 14:00, 17:00, and 20:00) for mobile observations. These specific times were chosen to comprehensively assess the impact of heat rejection from air-conditioning systems on the urban blocks' thermal environment. These times correspond to varying solar radiation intensities and human activity levels, providing a more accurate reflection of thermal environment changes throughout the day. The observer carried a portable temperature and humidity data logger along with a handheld GPS, identical to the one used for measuring air-conditioning heat rejection. At each selected time, the observer began at the Xiangjiang River, driving along the designated route at a constant speed and recording thermal and humidity data while tracking the location in real-time. Each testing round lasted about 40 min, with consecutive measurements taken throughout the week. Figure 5 illustrates the setup of the mobile measurement platform and the fixed weather stations.

Figure 5. The setting of mobile measurements. The left half of the picture shows a mobile measuring platform; the right half of the picture shows a weather station.

2.3.3. Correlation Analysis

Correlation analysis is a statistical method used for exploring the strength and direction of the relationship between two or more variables. It is primarily used to measure the strength of a linear relationship between two random variables. This paper focused on the use of Pearson's linear correlation method in exploring the relationship between air-conditioning heat rejection and the thermal and humid environment of a building area [19]. The equation can be expressed as follows:

$$R = \frac{n(\sum XY - (\sum X) \cdot (\sum Y)}{\sqrt{n\left(\sum X^2\right) - (\sum X)^2}\sqrt{n\left(\sum Y^2\right) - (\sum Y)^2}} \tag{1}$$

where n represents the number of observations; X represents the measures of variable 1; Y represents the measures of variable 2; $\sum XY$ represents the sum of the product of the respective variable measures; $\sum X$ represents the sum of the measures of variable 1; $\sum Y$ represents the sum of the measures of variable 2; $\sum X^2$ represents the sum of the squared values of the measures of variable 1; and $\sum Y^2$ represents the sum of the squared values of the measures of variable 2.

2.3.4. Temporal Corrections for Mobile Data

During the mobile testing, the thermal and humidity parameters at the measurement points were influenced by variations in the background meteorological conditions, leading to a lack of simultaneity in the collected data. To facilitate spatial comparisons, the observational data were adjusted to specific times. This study applied temperature and humidity correction formulas, as described in the referenced model [20], to adjust the recorded temperatures and humidity to correspond to the following times: 10:00, 14:00, 17:00, and 20:00. This adjustment provided a higher temporal resolution for characterizing the spatial and temporal distribution of the thermal environment. The model included multiple fixed weather stations as reference points and considered distance factors to improve the accuracy of the simultaneity corrections used for the mobile observational data. This study utilized benchmark reference data from four meteorological stations, collected at the specified testing times of 10:00, 14:00, 17:00, and 20:00. The equation can be expressed as:

$$y_{j,\ tr} - y_{j,\ tj} = \sum_{i=1}^{N}\left(x_{i,\ tr} - x_{i,\ tj}\right) \cdot l_{ij}^{-2} / \sum_{i=1}^{N} l_{ij}^{-2} \tag{2}$$

where $y_{j,tr}$ and $x_{i,tr}$ represent the thermal and moisture environmental parameters of the jth moving measuring point and the ith fixed measuring point at the unified correction time (tr), respectively; $y_{j,tj}$ and $x_{i,tj}$ represent the thermal and humid environment parameter values of the jth moving point and the ith fixed point at any time (tj) during the moving observation period, respectively; N represents the number of fixed meteorological stations; and l_{ij} represents the actual distance between the jth mobile station and the ith fixed station.

2.3.5. ArcGIS Spatial Visualization

In monitoring the thermal and humidity environment of urban neighborhoods, the mobile testing range-imposed limitations result in data collection from discrete, non-continuous measurement points along the route. To analyze the spatial distribution of the thermal parameters within the study area, spatial interpolation methods in ArcGIS were utilized to transform point data into block-level data, facilitating further spatial scale transformations.

Spatial interpolation, as described in reference [20], estimates unknown data for spatial points or areas based on known data. Previous research has demonstrated that

ordinary kriging is particularly effective for the precise interpolation of micro-scale thermal environment observation data [21]. With the kriging method [22], weights are calculated based on the distance between known and unknown points, as well as the spatial auto-correlation of the parameter variables. This method is grounded in variogram theory, which posits that the surface or volume of interest can be estimated using spatial covariance and the semivariogram functions. It provides a linear, unbiased, and optimal estimation of unknown parameter values, using original variable values and variogram properties. The expression for the semivariogram is based on the sampling data and the assumption of stationarity, and it is presented in equation form as follows:

$$\hat{Z}(x_0) = \sum_{i=1}^{N} \lambda_i Z(x_i) \tag{3}$$

$$\begin{cases} \sum_{i=1}^{N} \lambda_i C(x_i, x_j) + \mu = C(x_0, x_j)(j = 1, 2, \ldots, n) \\ \sum_{i=1}^{N} \lambda_i = 1 \end{cases} \tag{4}$$

where $Z(x_i)$ represents the measured value at the ith position; x_0 represents the predicted location; N represents the number of measured location points; λ_i represents the undetermined weight coefficient of the measured value at the ith position; and $C(x_0, x_j)$ represents the covariance function between x_i and x_j.

3. Results

3.1. Heat Rejection from Air-Conditioning Systems

The primary air-conditioning systems in commercial and residential buildings were monitored over a seven-day period, along with the atmospheric temperature and humidity measurements for comparison. Data from the temperature and humidity measurement instruments were exported to obtain information on heat rejection from different air-conditioning systems as well as the atmospheric temperature and humidity. Due to equipment damage during measurements, only three complete consecutive days (12–14 August) were selected for analysis. The temperature results of this monitoring are presented in Figure 6.

As shown in Figure 6, in Case 1, the exhaust air temperature from the cooling tower in commercial buildings was approximately 2.4 °C higher than the atmospheric temperature recorded in the morning and evening. At these times, the air from the cooling tower outlet has a heating effect on the surrounding atmosphere. Conversely, during midday and the afternoon, the temperature of the cooling tower exhaust air is lower than the atmospheric temperature due to the increase in atmospheric temperature. As a result, the exhaust air temperature was about 2.2 °C lower than the atmospheric temperature. In Case 2, the exhaust air temperature from the outdoor units of residential buildings closely followed the trend of the atmospheric temperature, consistently remaining higher throughout the day. During the day, when air conditioning was in operation, the outdoor units produced sensible heat, with the temperature difference between the exhaust and the atmosphere averaging at about 5.2 °C. At night, as temperatures gradually decreased, the temperature difference between the outdoor units' exhaust air and the surrounding environment increased. Around midnight, as temperatures continued to drop and air-conditioning usage decreased, heat rejection from the units began to decline; however, exhaust air temperature remained higher than atmospheric temperature, with an average temperature difference of about 6.5 °C. Overall, the exhaust air temperature of the outdoor units significantly raised atmospheric temperature throughout the day, with a more pronounced effect at night. The temperature difference between the exhaust air from the outdoor units and the atmosphere was slightly greater than the results obtained from previous models simulating the impact of outdoor air-conditioning units on urban environments in cities such as Tokyo,

Phoenix, and Berlin. However, this finding aligns with the observed phenomenon of more pronounced temperature increases at night compared to during the day [23–25].
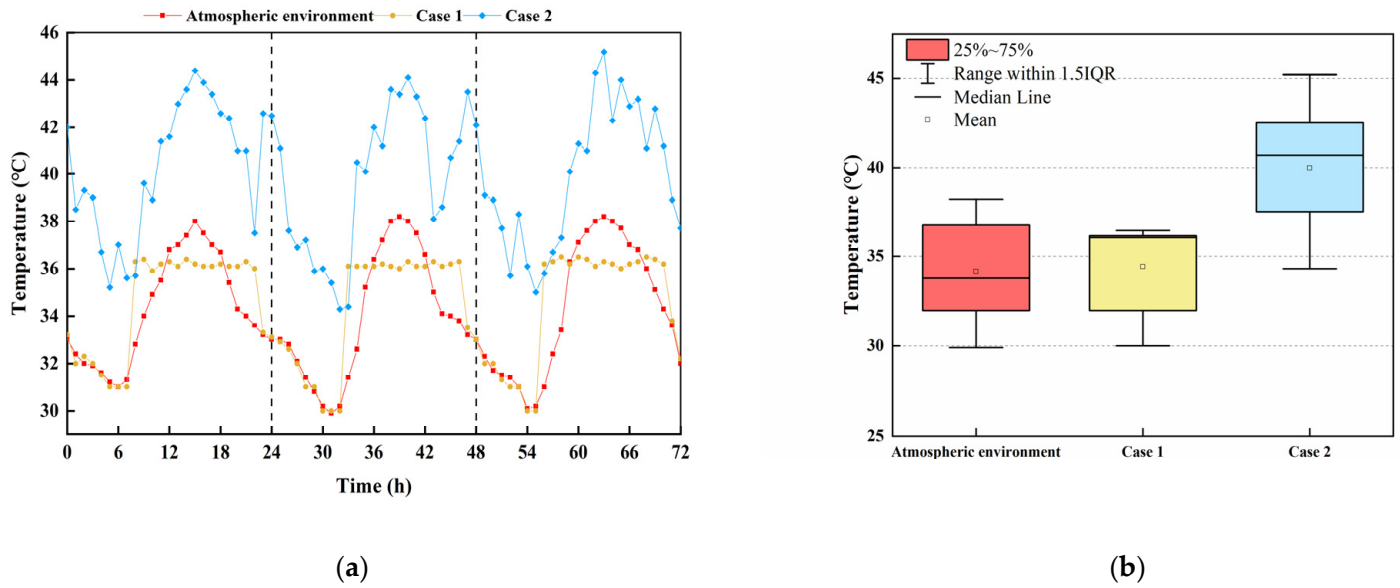

(**a**)   (**b**)

Figure 6. Changes in the temperature of the exhaust air from the air-conditioning system: (**a**) trends in the temperature of the exhaust air from the air-conditioning system; (**b**) range of variation in the temperature of the exhaust air from the air-conditioning system. Case 1 denotes the exhaust air temperature from the cooling towers of commercial buildings; Case 2 denotes the exhaust air temperature from the outdoor air-conditioning units of residential buildings.

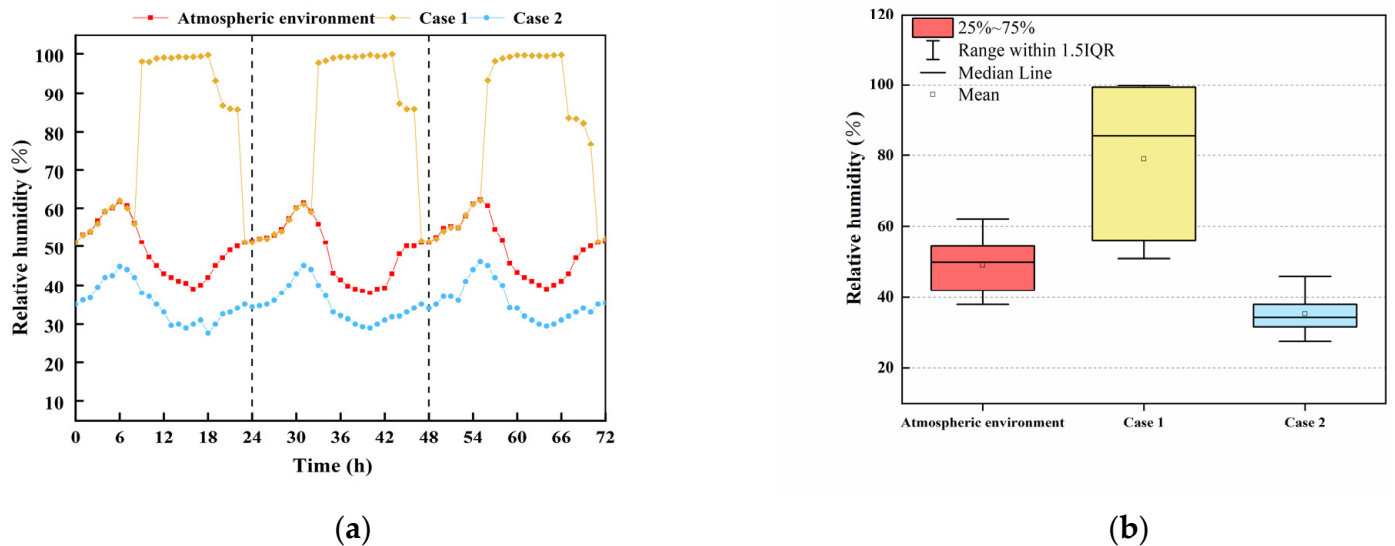The relative humidity results of this monitoring are presented in Figure 7.

(**a**)   (**b**)

Figure 7. Changes in relative the humidity of the exhaust air from the air-conditioning system: (**a**) trends in the humidity of the exhaust air from the air-conditioning system; (**b**) range of variation in the humidity of the exhaust air from the air-conditioning system. Case 1 denotes the exhaust air relative humidity from the cooling tower of commercial buildings; Case 2 denotes the exhaust air relative humidity from the outdoor air-conditioning units of residential buildings.

As shown in Figure 7, in Case 1, the cooling tower operated as an open system, facilitating heat and moisture exchange through the direct contact between water and air [26], primarily rejecting heat as latent heat [27]. During the day, the exhaust air relative humidity from the cooling tower remained between 95.2% and 99.8% due to its open

heat and moisture exchange system, being significantly higher than the average outdoor air relative humidity of 45.5%. In the evening, the relative humidity of the exhaust air from the cooling tower was 85.3%, still significantly higher than the atmospheric relative humidity of 58.5%. At night, when the cooling tower ceased operation, its relative humidity became comparable to that of the atmosphere, ranging from 50.3% to 62.5%. Consequently, the higher air-conditioning usage during the day caused the wet air discharged from the cooling tower to significantly influence the surrounding humidity, with a more pronounced effect during the day than at night. In contrast to the open system of cooling towers, in Case 2, the outdoor units operated in a closed-loop refrigerant cycle, without direct heat and mass exchange with outdoor air. Therefore, the moisture content of the exhaust air should theoretically match that of the atmospheric air. However, measured data indicated that the relative humidity of the exhaust air was consistently lower than that of the surrounding environment. This discrepancy was primarily due to air disturbance caused by the exhaust, which reduced the moisture content near the exhaust outlet by displacing surrounding water vapor, leading to lower relative humidity. Nonetheless, this localized effect did not significantly affect the overall surrounding humidity environment.

3.2. Correlation Analysis Between Air-Conditioning Heat Rejection and the Neighborhood Environment

To analyze the impact of different building air-conditioning systems' heat rejection on the neighborhood thermal environment, this study conducted an in-depth analysis of relevant measured data. We focused on several key variables as follows: the temperature difference between the outdoor unit and the atmosphere (ΔTa), the temperature difference between the residential building area of meteorological Station 2 and the suburban meteorological station ($\Delta T2$), the relative humidity difference between the cooling tower and the atmosphere (ΔRHc), and the relative humidity difference between the commercial building area meteorological Station 1 and the suburban meteorological station ($\Delta RH1$). The correlation analysis results are detailed in Figures 8 and 9, illustrating the relationships between the variables and the extent of their influence.
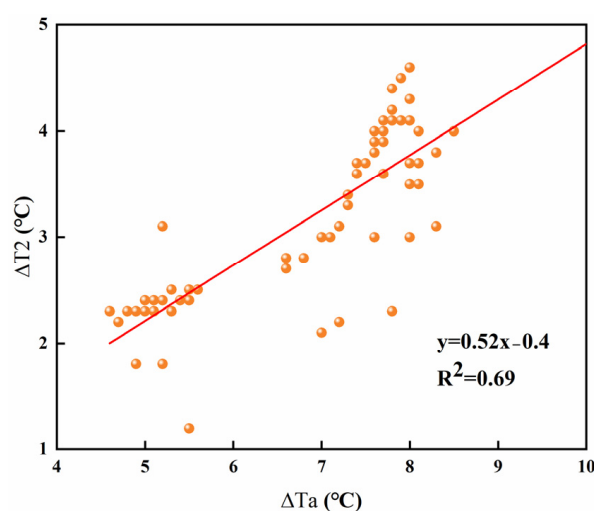

Figure 8. Linear relationship between ΔTa and $\Delta T2$. ΔTa denotes the temperature difference between the outdoor unit and the atmosphere; $\Delta T2$ denotes the temperature difference between the residential building area meteorological Station 2 and the suburban meteorological station.

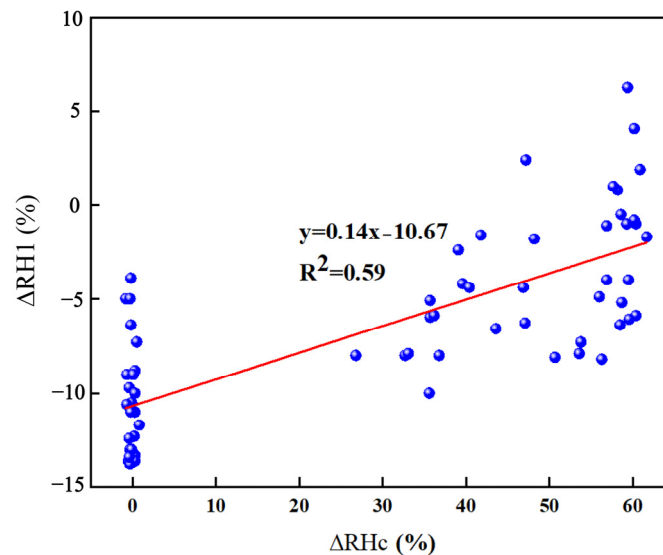**Figure 9.** Linear relationship between ΔRHc and ΔRH1. ΔRHc denotes the relative humidity difference between the cooling tower and the atmosphere; ΔRH1 denotes the relative humidity difference between the commercial building area meteorological Station 1 and the suburban meteorological station.

As shown in Figure 8, the correlation coefficient was 0.69, indicating a strong positive correlation between the heat exhaust of outdoor units and the temperature increase in the residential building area. This suggested that heat exhaust from outdoor air-conditioning units significantly affected the neighborhood thermal environment, highlighting the need to consider this effect in urban planning and construction. Meanwhile, Figure 8 shows a correlation coefficient of 0.59, indicating a positive correlation between the humidity exhaust of the cooling tower and the increase in relative humidity in commercial building areas, suggesting that this discharge affected neighborhood humidity.

It is important to note that the temperature and relative humidity of residential and commercial buildings were influenced by various factors, including traffic heat removal and heat-absorbing materials. However, this study identified air-conditioning heat rejection as a significant factor influencing the temperature and humidity of built-up areas, and this has to be considered in urban design and planning.

3.3. Temperature and Humidity Data with Spatiotemporal Correction

In this study, the obtained mobile measurements were corrected, and the correction results are shown in Figures 10 and 11.

As shown in Figures 10 and 11, there were obvious differences between the original test data and the corrected data at different test moments. Since the mobile test route was closed, the temperature and humidity at the starting and ending positions should theoretically have been the same or very similar. The figures showed that the temperature and humidity at the corrected starting and ending points were closely matched, while the data before correction exhibited a significant difference. Therefore, it was necessary to correct the data with respect to time and space.
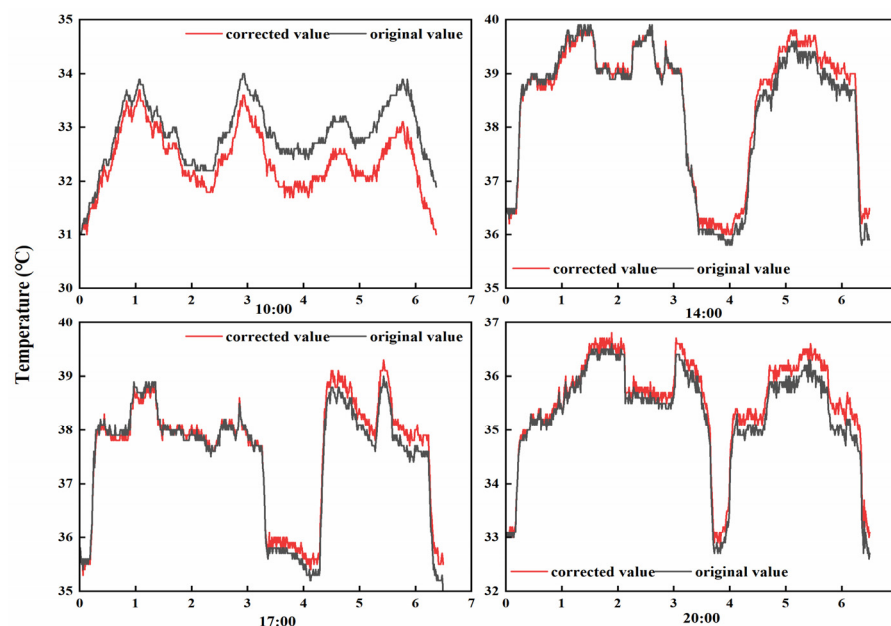
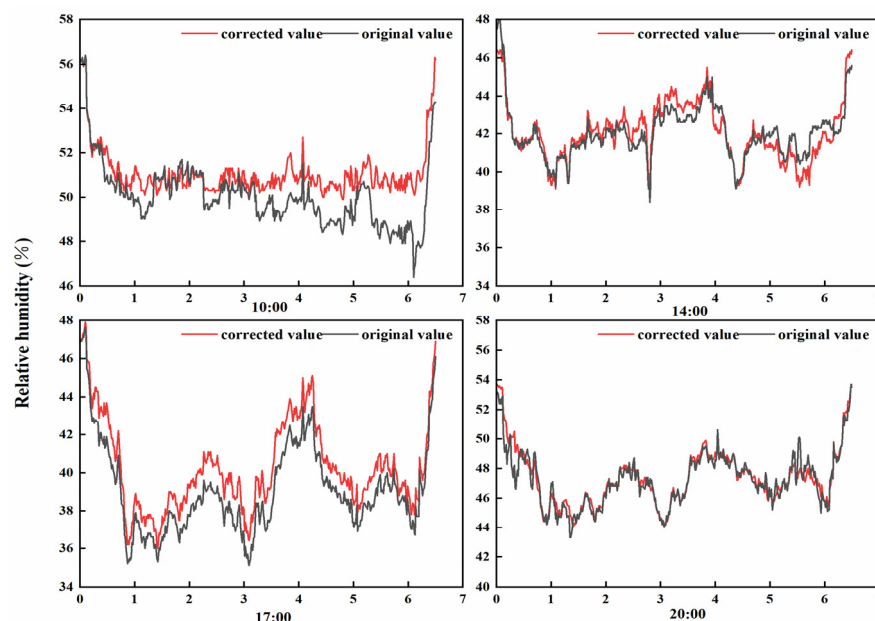**Figure 10.** Temperature correction for mobile test data.

Figure 11. Relative humidity correction for mobile test data.

3.4. Temperature and Humidity Distribution Along the Mobility Routes

To highlight the impact of different underlying surfaces and building types on the thermal environment of urban blocks, this study compared the corrected temperature and humidity values with hourly air temperature and humidity data from the suburbs, resulting in the average temperature differences (ΔT) and relative humidity differences (ΔRH) between the mobile route and the suburban area. The data were then imported into ArcGIS software to visualize the average values of temperature and humidity differences along the mobile route at various time points during the measurement period, as shown in Figures 12 and 13.

Figure 12. Distribution of temperature on mobile test routes. ΔT denotes the temperature differences between the mobile route and the suburban area.
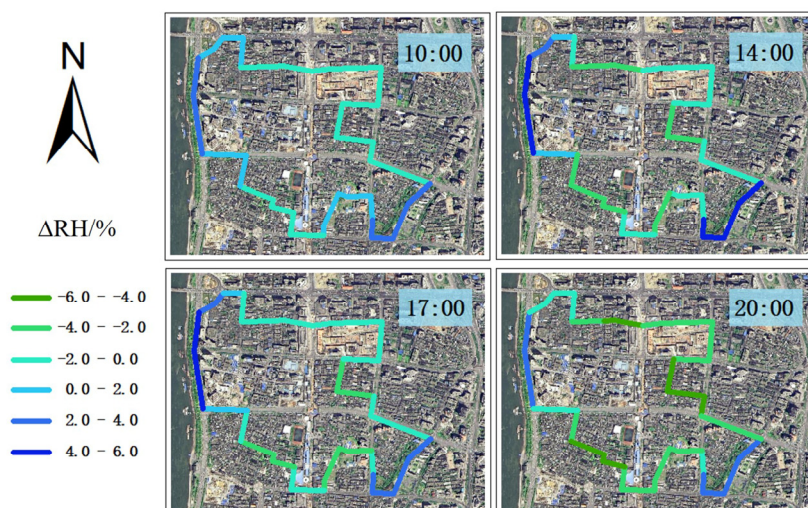

Figure 13. Distribution of relative humidity on mobile test routes. ΔRH denotes the relative humidity differences between the mobile route and the suburban area.

As shown in Figures 12 and 13, the temperature difference from the suburban areas in the Wuyi Square commercial area generally ranged from $-1.5\ °C$ to $3.0\ °C$ at different times, while the relative humidity difference varied from -6% to 6%. There are obvious differences in the temperature and humidity differences in different underlying surface areas and building types.

In terms of temporal distribution, the temperature difference from suburban areas in the riverside and park areas along the mobile route ranged from $-0.5\ °C$ to $0\ °C$ in the morning, $-1.5\ °C$ to $-0.5\ °C$ in the afternoon, and $-1.0\ °C$ to $0\ °C$ in the evening. The relative humidity differences ranged from 2% to 4% in the morning, 4% to 6% in the afternoon, and 2% to 4% in the evening. These variations were mainly due to the reduced solar radiation in the morning and evening, which decreased the heat absorption and humidification capacity of riverside water and park vegetation. In the afternoon, when solar radiation was strongest, the heat and humidity absorption capacity of these elements peaked. Consequently, the temperature difference from suburban areas in the riverside and park areas was approximately $0.5\ °C$ lower in the afternoon compared to the morning and evening, while the relative humidity difference was about 2% higher. In contrast, the temperature difference from suburban areas in commercial and residential zones ranged

from 1 °C to 2 °C in the morning, 1.0 °C to 2.5 °C in the afternoon, and 2.0 °C to 3.0 °C in the evening. The relative humidity differences ranged from −2.0% to 0% in the morning, −4.0% to −2.0% in the afternoon, and −6.0% to −2.0% in the evening. The differences in temperature and humidity over time between the commercial and residential zones were largely driven by human activity. In the morning, lower outdoor temperatures and decreased occupancy rates resulted in reduced air-conditioning energy consumption and lower sensible heat rejection. In the afternoon, rising outdoor temperatures increased air-conditioning usage, enhancing sensible heat rejection and raising the temperature difference. In the evening, increased occupancy rates caused air conditioning to operate at peak levels, resulting in the highest heat exchange with the outdoor environment and the greatest temperature difference [28,29].

In terms of spatial distribution, significant differences in temperature and humidity were observed along the mobile routes in the Wuyi Square commercial area. The riverside and park areas along the route exhibited temperatures lower than those in suburban areas, ranging from −1.5 °C to 0 °C, while the relative humidity was higher by 2.0% to 6.0%. In contrast, the commercial and residential areas exhibited temperatures higher than those in suburban areas, ranging from 0.5 °C to 3.0 °C, with relative humidity levels lower by 2.0% to 6.0%. These differences primarily arose from the characteristics of the underlying surfaces. The riverside area contained water, while the park area was predominantly vegetated, both exhibiting good heat absorption and humidity-enhancing properties. Conversely, the commercial and residential zones were mainly composed of low-reflectance asphalt surfaces, which have a high heat absorption and storage capacity, contributing to the increased temperatures in the surrounding environment. This aligned with findings from previous studies [30–32]. Additionally, significant air-conditioning condensation heat and traffic waste heat were difficult to dissipate in narrow streets, leading to elevated temperatures and reduced humidity in these areas. Together, these factors contributed to the significant differences in temperature and humidity across different regions.

3.5. Spatial Distribution of Temperature and Humidity

The measured data were imported into ArcGIS to extract masks within the Wuyi Square commercial area. This created spatial visualizations of temperature and relative humidity at 10:00, 14:00, 17:00, and 20:00, as shown in Figures 14 and 15.
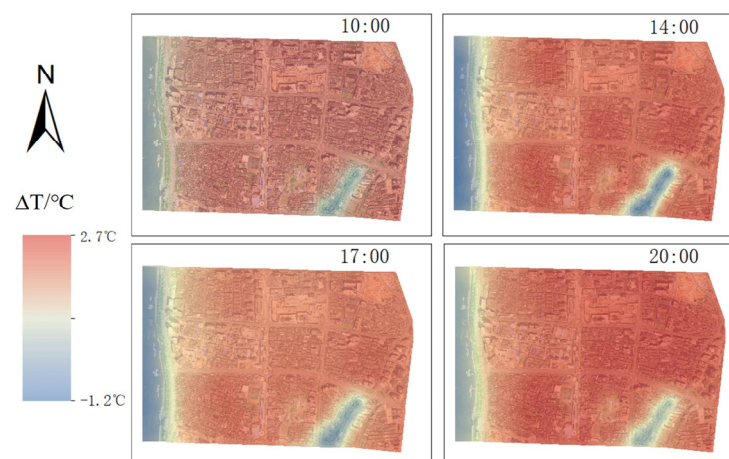

Figure 14. Spatial and temporal distribution of temperature. ΔT denotes the temperature differences between the study area and the suburban area.
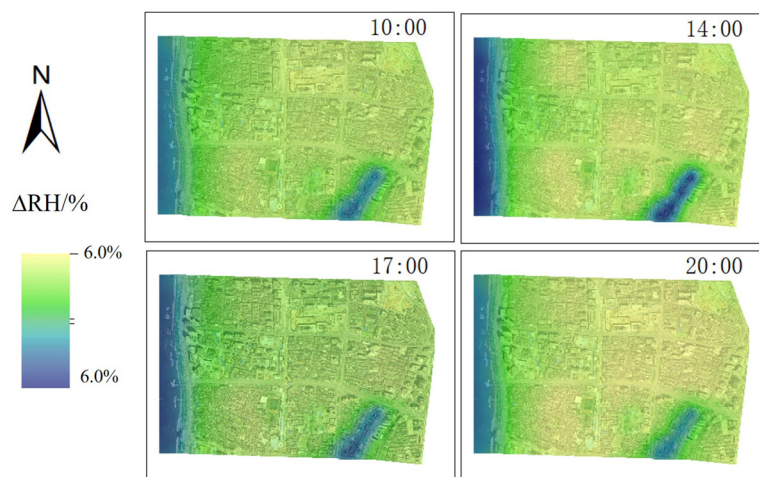
Figure 15. Spatial and temporal distribution of relative humidity. ΔRH denotes the relative humidity differences between the study area and the suburban area.

The temperature difference between the urban area and the suburbs in the Wuyi Square commercial area generally ranged from −1.2 °C to 2.7 °C, while the relative humidity difference fell between −6.0% and 6.0%. Average temperature and humidity parameters for each neighborhood were calculated using the "partition statistics" tool in ArcGIS, as shown in Tables 1 and 2 and Figure 16.

Table 1. The average temperature difference (°C) of each zone throughout the day. Zones 1, 3, 5, 6, 7, and 8 mainly consisted of residential buildings, while Zones 2 and 4 were primarily commercial. Zone 10 featured water as the primary underlying surface, while Zone 9 included vegetation along with some residential buildings.

Region	10:00	14:00	17:00	20:00	Average
Zone 1	1.6	1.9	1.9	1.9	1.8
Zone 2	1.9	2.21	1.9	2.3	2.0
Zone 3	2.2	2.3	2.2	2.5	2.3
Zone 4	1.7	1.8	1.8	1.8	1.8
Zone 5	2.2	2.4	2.2	2.6	2.4
Zone 6	2.2	2.5	2.2	2.6	2.4
Zone 7	1.9	2.2	1.9	2.4	2.1
Zone 8	2.0	2.2	1.9	2.4	2.1
Zone 9	1.0	1.1	1.1	1.1	1.1
Zone 10	−0.6	−1.0	−0.9	−0.5	−0.8
Average	1.6	1.8	1.6	1.9	

Table 2. The average humidity difference (%) of each zone throughout the day.

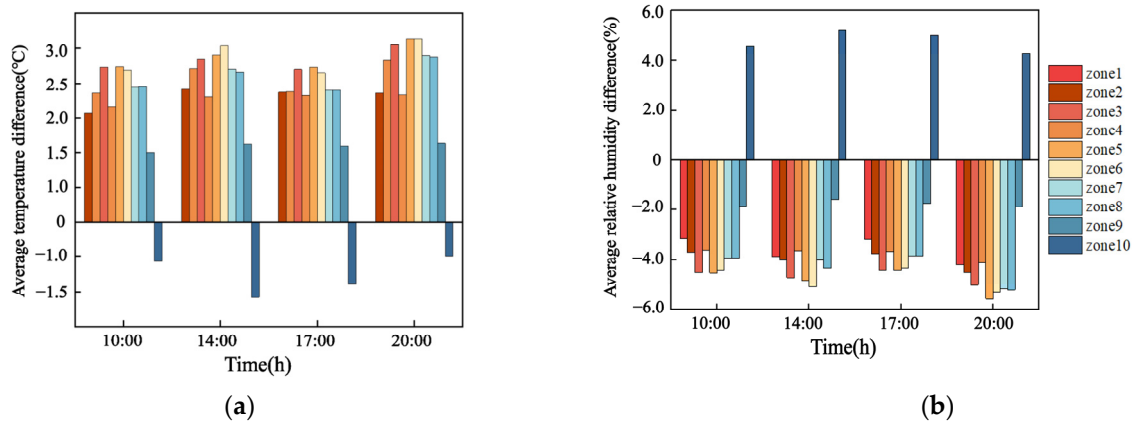| Region	10:00	14:00	17:00	20:00	Average
Zone 1	−3.2	−3.9	−3.2	−4.2	−3.6
Zone 2	−3.7	−4.0	−3.8	−4.5	−4.0
Zone 3	−4.5	−4.7	−4.4	−5.0	−4.7
Zone 4	−3.6	−3.6	−3.7	−4.1	−3.8
Zone 5	−4.5	−4.8	−4.4	−5.6	−4.8
Zone 6	−4.4	−5.1	−4.3	−5.3	−4.8
Zone 7	−3.9	−4.0	−3.8	−5.2	−4.2
Zone 8	−3.9	−4.4	−3.8	−5.2	−4.3
Zone 9	−1.9	−1.6	−1.8	−1.9	−1.8
Zone 10	4.6	5.2	5.0	4.3	4.8
Average	−2.9	−3.1	−2.8	−3.7	

Figure 16. Average temperature and humidity difference in the neighborhood thermal environment. (**a**) Average temperature difference in the thermal environment of the neighborhood; (**b**) Average relative humidity difference in the thermal environment of the neighborhood.

In terms of temporal distribution, the average temperature difference between the urban area and the suburbs in the test area was measured at 1.6 °C, 1.8 °C, 1.6 °C, and 1.9 °C at different times of the day. The average relative humidity difference ranged from −2.9% to −3.7%. In the morning, low air-conditioning usage and cooler temperatures led to minimal heat rejection. In the afternoon, peak outdoor temperatures increased air-conditioning energy consumption, worsening the outdoor temperature and humidity conditions. By evening, peak air-conditioning usage intensified the temperature difference with the suburbs. In the commercial building area, the mean temperature difference with the suburbs was approximately 2.0 °C during the day and increased to 2.1 °C at night, reflecting a difference of about 0.1 °C. Air exhausts from cooling towers lowered the environmental temperature during the day but raised it at night. In residential areas, the mean temperature difference with the suburbs was around 2.0 °C during the day and rose to 2.6 °C at night, reflecting a 0.6 °C increase due to the higher nighttime air-conditioning usage and sensible heat discharge, further elevating environmental temperature.

In terms of spatial distribution, the average temperature differences between the urban area and the suburbs at the riverside (Zone 10) and park area (Zone 9) were −0.8 °C and 1.1 °C, respectively, which are significantly lower than in other regions. The average relative humidity differences were 4.8% and −1.8%, respectively, which are much higher than in other areas. This can be attributed to the natural surface's ability to absorb heat and enhance humidity, as well as the distance from air-conditioning heat rejection. Areas with cement and asphalt surfaces also show variations in temperature and humidity. The riverside zones (Zone 1, Zone 4, Zone 7) had average temperature differences of 1.8 °C, 1.8 °C, and 2.1 °C, respectively, which are lower than the comparable areas. Their average relative humidity differences were −3.6%, −3.8%, and −4.2%, respectively, which are higher than in other regions. This cooling effect is influenced by nearby rivers, which lower temperatures and increase humidity [33]. In commercial building areas (Zone 2 and Zone 4), temperatures were approximately 0.3 °C lower than in residential areas (Zone 5, Zone 6, Zone 8). However, the relative humidity in Zones 2 and 4 was about 0.5% higher. This difference is primarily due to the use of cooling towers in commercial buildings, which release latent heat and enhance humidity during the day. In contrast, residential buildings primarily use split-system air conditioning, which contributes to higher surrounding temperatures.

4. Discussion

4.1. The Impact of Air-Conditioning Heat Rejection and the Underlying Surfaces

The rapid adoption and the increasing use of air-conditioning systems has notably affected urban thermal environments. Although numerous studies have examined the effects of air-conditioning heat rejection, most have focused on general assessments without differentiating between unit types or analyzing their specific impact on outdoor temperature and humidity. This study utilized field measurements and GIS spatial analysis, focusing on the commercial area of Wuyi Square in Changsha. We assessed the impact of air-conditioning heat rejection on the thermal and humidity environment of the district, analyzing variations across different building types and natural surfaces under the influence of air-conditioning rejection. This study enhances the understanding of the mechanisms behind air-conditioning heat rejection in urban thermal environments. It serves as a crucial reference for future urban planning, air-conditioning system design, and improvements to the thermal environment.

This study revealed that air-conditioning heat rejection significantly affects outdoor temperature and humidity, which is consistent with the existing literature [25,34,35]. Previous research has largely centered on UHI effects, often overlooking the differences among various types of air-conditioning heat rejection. This study further categorized and examined the distinct effects of various air-conditioning heat rejection systems, both on environmental temperature and humidity. Additionally, this research explored correlations between air-conditioning heat rejection and temperature or humidity across different building types. It found that the moisture released from cooling towers correlates with the humid environment of commercial areas, while heat rejection from outdoor units is strongly correlated with the temperature of residential areas. These findings further validated that air-conditioning heat rejection is a significant factor in altering outdoor thermal and humid environments, thereby supplementing and extending existing research. Furthermore, by comparing different building areas with unaffected natural underlying sur-faces, such as water and green spaces, we observed that these surfaces exhibited lower temperatures and higher humidity, with water providing a stronger cooling effect than green spaces. This conclusion is consistent with previous studies [36–38]. However, those studies mainly focused on the humidifying and cooling effects of green spaces and water, without comparing them to areas impacted by air-conditioning heat rejection. Our research highlights the critical role of green spaces and water in alleviating the effects of air-conditioning heat rejection. Studies on river cooling effects have indicated that river segments adjacent to green spaces show enhanced cooling effects [39]. In our study area, however, water and green spaces were not in close proximity, indicating opportunities for future research on their combined effects in mitigating air-conditioning heat rejection. Urban planners should incorporate these findings to consider the interactions between various building types and their surrounding environments in air-conditioning system designs, aiming for the more effective thermal management and mitigation of UHI effects.

4.2. Improving the Urban Thermal Environment

The significant increase in air-conditioning usage resulted in substantial heat rejection into the outdoor atmosphere, exacerbating the urban thermal climate issues [23–25,40]. This intensification degraded the thermal environment around buildings, necessitating the prolonged operation of air-conditioning systems to maintain indoor comfort, thus increasing their thermal load [16,41]. Consequently, more heat was released into the urban atmosphere in both sensible and latent forms, creating a vicious cycle that exacerbates urban thermal challenges.

To optimize the urban thermal environment regarding air-conditioning heat rejection in different building types, three approaches can be considered, involving altering building density, modifying building layout [42,43], and utilizing waste heat from air-conditioning systems as follows: (1) Increase overall building density. This enhances ventilation along main roads, leading to noticeable improvements in residual heat and moisture from air conditioning. (2) Modifying building layout. Arranging buildings in parallel or staggered patterns can create ventilation corridors, effectively dispersing heat emitted by air-conditioning systems and preventing heat accumulation. (3) Utilizing waste heat recovery technology [44,45]. Waste heat from air-conditioning systems can be harnessed for various purposes, such as domestic hot water supply, winter heating, or nearby industrial processes.

From the perspective of different underlying surfaces, the urban thermal environment can be optimized by focusing on the following two aspects: (1) Increasing water areas. This can be achieved by constructing artificial lakes or reservoirs and developing wetland parks in low-lying urban areas. (2) Increasing green space areas. Existing parks and green spaces can be enlarged, and greening efforts can be extended to overpasses, elevated bridges, public buildings, and residential rooftops to enhance vertical greenery coverage.

4.3. Limitations and Prospects

This study examines the impact of building air-conditioning heat rejection and surface materials on the thermal climate of urban neighborhoods, offering valuable insights for mitigating urban thermal environments. However, the current research has some limitations.

First, while field measurements provide authentic data, they require substantial human and material resources and are limited by weather conditions. Second, the analysis mainly considers the horizontal effects of air-conditioning heat rejection and surface materials on the urban thermal environment, with insufficient discussion on vertical height. Lastly, there has been insufficient investigation into the regulatory mechanisms of the urban thermal environment.

Therefore, future research should focus on the following areas: (1) Integrating advanced techniques, such as numerical simulation and remote sensing, to accurately analyze how building air-conditioning heat rejection and different surface types influence surface temperature; (2) Expanding the research perspective beyond the 1.5 m pedestrian height limitation to conduct comprehensive spatiotemporal analyses of air-conditioning heat rejection; (3) Exploring effective strategies for mitigating the urban thermal climate from the perspectives of both building air-conditioning heat rejection and surface material.

5. Conclusions

This study presented field measurements conducted in the Wuyi Square commercial district in Changsha, discussing the temporal distribution patterns of heat rejection from air-conditioning systems across various building types and its impact on the neighborhood's thermal environment. Using ArcGIS technology, this study visualized the thermal and humidity environment on the block scale and analyzed the spatiotemporal patterns of thermal and humidity parameters of different underlying surfaces, considering air-conditioning heat rejection. The key findings of this investigation are as follows:

The cooling towers of air-conditioning systems in public buildings significantly increase the humidity of the surrounding environment. The relative humidity of the exhaust air from these cooling towers during the day fluctuates between 95.2% and 99.8%. Conversely, the outdoor units of split-type air conditioners in residential buildings notably raise the temperature of the surrounding environment. The exhaust air temperatures from these

units are, on average, 5.2 °C higher during the day and 6.5 °C higher at night compared to the respective outdoor ambient temperatures.

Spatial analysis indicated that the average temperature difference between the green space and water area and the suburban area is 1.1 °C and −0.8 °C, respectively, which is significantly lower than that of the built-up area. Meanwhile, the average relative humidity difference between these areas is −1.8% and 4.8%, which is significantly higher than that of the built-up areas, and the mitigating effect of green spaces and water on air-conditioning heat exhaust rejection is obvious. Furthermore, due to variations in air-conditioning usage and heat rejection systems, commercial areas had an average temperature that is approximately 0.3 °C lower than that of residential areas, highlighting differences in the thermal environment between various building types. These findings provide important references for future urban planning and air-conditioning system design.

References

1. Sharmin, T.; Chappell, A.; Lannon, S. Spatio-temporal analysis of LST, NDVI and SUHI in a coastal temperate city using local climate zone. *Energy Built Environ.* **2024**. [CrossRef]
2. Kou, Y.; Xian, D.; Liu, Y.; Chen, J.; Wang, C.; Cheng, B.; Guo, W.; Li, Y.; Tang, L. Factors affecting urban climate at different times of the day in China: A case study in Yibin, a riverside mountain city. *Nat.-Based Solut.* **2022**, *2*, 100043. [CrossRef]
3. Yuan, C.; Adelia, A.S.; Mei, S.; He, W.; Li, X.-X.; Norford, L. Mitigating intensity of urban heat island by better understanding on urban morphology and anthropogenic heat dispersion. *Build. Environ.* **2020**, *176*, 106876. [CrossRef]
4. He, W.; Li, X.-X.; Zhang, X.; Yin, T.; Norford, L.K.; Yuan, C. Estimation of anthropogenic heat from buildings based on various data sources in Singapore. *Urban Clim.* **2023**, *49*, 101434. [CrossRef]
5. Chen, W.; Zhou, Y.; Xie, Y.; Chen, G.; Ding, K.J.; Li, D. Estimating spatial and temporal patterns of urban building anthropogenic heat using a bottom-up city building heat emission model. *Resour. Conserv. Recycl.* **2022**, *177*, 105996. [CrossRef]
6. Lu, S.; Qi, Y.; Cai, Z.; Li, Y. Optimization model analysis of centralized groundwater source heat pump system in heating season. *Front. Energy* **2015**, *9*, 343–361. [CrossRef]
7. Cui, J.; Xie, L.; Zheng, X. Climate change, air conditioning, and urbanization—Evidence from daily household electricity consumption data in China. *Clim. Chang.* **2023**, *176*, 106. [CrossRef]
8. Chen, Q.; Yang, X.; Ouyang, Z.; Zhao, N.; Jiang, Q.; Ye, T.; Qi, J.; Yue, W. Estimation of anthropogenic heat emissions in China using Cubist with points-of-interest and multisource remote sensing data. *Environ. Pollut.* **2020**, *266*, 115183. [CrossRef]
9. Hsieh, C.-M.; Aramaki, T.; Hanaki, K. The feedback of heat rejection to air conditioning load during the nighttime in subtropical climate. *Energy Build.* **2007**, *39*, 1175–1182. [CrossRef]
10. Sun, Y.; Augenbroe, G. Urban heat island effect on energy application studies of office buildings. *Energy Build.* **2014**, *77*, 171–179. [CrossRef]
11. Liu, K.; Du, Y.; Chen, W.; Wu, X. Simulation of interaction between high-temperature process and heat emission from electricity system in summer. *Glob. Energy Interconnect.* **2022**, *5*, 692–702. [CrossRef]

12. Yang, L.; Qian, F.; Song, D.-X.; Zheng, K.-J. Research on urban heat-island effect. *Procedia Eng.* **2016**, *169*, 11–18. [CrossRef]

13. Toparlar, Y.; Blocken, B.; Maiheu, B.; van Heijst, G.J.F. A review on the CFD analysis of urban microclimate. *Renew. Sustain. Energy Rev.* **2017**, *80*, 1613–1640. [CrossRef]

14. Wetherley, E.B.; Roberts, D.A.; Tague, C.L.; Jones, C.; Quattrochi, D.A.; McFadden, J.P. Remote sensing and energy balance modeling of urban climate variability across a semi-arid megacity. *Urban Clim.* **2021**, *35*, 100757. [CrossRef]

15. Meng, F.; Ren, G.; Zhang, R. Impacts of UHI on Heating and Cooling Loads in Residential Buildings in Cities of Different Sizes in Beijing–Tianjin–Hebei Region in China. *Atmosphere* **2023**, *14*, 1193. [CrossRef]

16. Tariku, F.; Gharib Mombeni, A. ANN-Based Method for Urban Canopy Temperature Prediction and Building Energy Simulation with Urban Heat Island Effect in Consideration. *Energies* **2023**, *16*, 5335. [CrossRef]

17. Zhong, X.; Cai, M.; Wang, Z.; Zhang, Z.; Zhang, R. Influences of Heat Rejection from Split A/C Conditioners on Mixed-Mode Buildings: Energy Use and Indoor Air Pollution Exposure Analysis. *Buildings* **2024**, *14*, 318. [CrossRef]

18. Kousis, I.; Pigliautile, I.; Pisello, A.L. Intra-urban microclimate investigation in urban heat island through a novel mobile monitoring system. *Sci. Rep.* **2021**, *11*, 9732. [CrossRef]

19. Senthilnathan, S. Usefulness of Correlation Analysis. 2019. Available online: https://ssrn.com/abstract=3416918 (accessed on 12 January 2025).

20. Liu, L.; Pan, X.; Jin, L.; Liu, L.; Liu, J. Association analysis on spatiotemporal characteristics of block-scale urban thermal environments based on a field mobile survey in Guangzhou, China. *Urban Clim.* **2022**, *42*, 101131. [CrossRef]

21. Getis, A.; Ord, J.K. The analysis of spatial association by use of distance statistics. *Geogr. Anal.* **1992**, *24*, 189–206. [CrossRef]

22. Dobesch, H.; Dumolard, P.; Dyras, I. *Spatial Interpolation for Climate Data: The Use of GIS in Climatology and Meteorology*; John Wiley & Sons: Hoboken, NJ, USA, 2013.

23. Ohashi, Y.; Genchi, Y.; Kondo, H.; Kikegawa, Y.; Yoshikado, H.; Hirano, Y. Influence of air-conditioning waste heat on air temperature in Tokyo during summer: Numerical experiments using an urban canopy model coupled with a building energy model. *J. Appl. Meteorol. Climatol.* **2007**, *46*, 66–81. [CrossRef]

24. Salamanca, F.; Georgescu, M.; Mahalov, A.; Moustaoui, M.; Wang, M. Anthropogenic heating of the urban environment due to air conditioning. *J. Geophys. Res. Atmos.* **2014**, *119*, 5949–5965. [CrossRef]

25. Jin, L.; Schubert, S.; Hefny Salim, M.; Schneider, C. Impact of air conditioning systems on the outdoor thermal environment during summer in Berlin, Germany. *Int. J. Environ. Res. Public Health* **2020**, *17*, 4645. [CrossRef] [PubMed]

26. Mishra, B.; Srivastava, A.; Yadav, L. Performance analysis of cooling tower using desiccant. *Heat Mass Transf.* **2020**, *56*, 1153–1169. [CrossRef]

27. Han, M.; Chen, H. Effect of external air-conditioner units' heat release modes and positions on energy consumption in large public buildings. *Build. Environ.* **2017**, *111*, 47–60. [CrossRef]

28. Mori, H.; Kubota, T.; Antaryama, I.G.N.; Ekasiwi, S.N.N. Analysis of window-opening patterns and air conditioning usage of urban residences in tropical southeast Asia. *Sustainability* **2020**, *12*, 10650. [CrossRef]

29. Liu, M.; Zhai, Y.; Qiu, X.; Xie, X.; Liu, Z.; Zhu, L.; Lei, Y.; Li, Z. Air-conditioning usage behaviour of the elderly in caring home during the extremely hot summer period: An evidence in Chongqing. *Build. Environ.* **2023**, *244*, 110828. [CrossRef]

30. Lai, S.; Zhao, Y.; Fan, Y.; Ge, J. Characteristics of daytime land surface temperature in wind corridor: A case study of a hot summer and warm winter city. *J. Build. Eng.* **2021**, *44*, 103370. [CrossRef]

31. Jian, L.; Xia, X.; Wang, Y.; Liu, X.; Zhang, Y.; Yang, Q. Spatiotemporal dynamic relationships and simulation of urban spatial form changes and land surface temperature: A case study in Chengdu, China. *Front. Public Health* **2024**, *12*, 1357624. [CrossRef]

32. Zhang, J.; Zhu, G.; Yin, J.; Ma, J.; Kong, X. Analysis of summer high temperature observations based on different sub surfaces. *Earth Sci. Inform.* **2024**, *17*, 5095–5105. [CrossRef]

33. Wang, Y.; Ouyang, W.; Zhan, Q.; Zhang, L. The cooling effect of an urban river and its interaction with the littoral built environment in mitigating heat stress: A mobile measurement study. *Sustainability* **2022**, *14*, 11700. [CrossRef]

34. Schulze, C.; Raabe, B.; Herrmann, C.; Thiede, S. Environmental impacts of cooling tower operations–The influence of regional conditions on energy and water demands. *Procedia CIRP* **2018**, *69*, 277–282. [CrossRef]

35. Wang, Y.; Li, Y.; Sabatino, S.D.; Martilli, A.; Chan, P. Effects of anthropogenic heat due to air-conditioning systems on an extreme high temperature event in Hong Kong. *Environ. Res. Lett.* **2018**, *13*, 034015. [CrossRef]

36. Aram, F.; García, E.H.; Solgi, E.; Mansournia, S. Urban green space cooling effect in cities. *Heliyon* **2019**, *5*, e01339. [CrossRef] [PubMed]

37. Xie, Q.; Ren, L.; Yang, C. Regulation of water bodies to urban thermal environment: Evidence from Wuhan, China. *Front. Ecol. Evol.* **2023**, *11*, 983567. [CrossRef]

38. Xu, H.; Sheng, K.; Gao, J. Mitigation of heat island effect by green stormwater infrastructure: A comparative study between two diverse green spaces in Nanjing. *Front. Ecol. Evol.* **2023**, *11*, 1307756. [CrossRef]

39. Zhou, W.; Wu, T.; Tao, X. Exploring the spatial and seasonal heterogeneity of cooling effect of an urban river on a landscape scale. *Sci. Rep.* **2024**, *14*, 8327. [CrossRef]

40. Österreicher, D.; Sattler, S. Maintaining comfortable summertime indoor temperatures by means of passive design measures to mitigate the urban heat island effect—A sensitivity analysis for residential buildings in the City of Vienna. *Urban Sci.* **2018**, *2*, 66. [CrossRef]

41. Wang, S.; Wang, Z.; Zhang, Y.; Fan, Y. Characteristics of urban heat island in China and its influences on building energy consumption. *Appl. Sci.* **2022**, *12*, 7678. [CrossRef]

42. Kolokotsa, D.; Lilli, K.; Gobakis, K.; Mavrigiannaki, A.; Haddad, S.; Garshasbi, S.; Mohajer, H.R.H.; Paolini, R.; Vasilakopoulou, K.; Bartesaghi, C. Analyzing the impact of urban planning and building typologies in urban heat island mitigation. *Buildings* **2022**, *12*, 537. [CrossRef]

43. Li, Y.; Schubert, S.; Kropp, J.P.; Rybski, D. On the influence of density and morphology on the Urban Heat Island intensity. *Nat. Commun.* **2020**, *11*, 2647. [CrossRef] [PubMed]

44. Lamrani, B.; El Marbet, S.; Rehman, T.-u.; Kousksou, T. Comprehensive analysis of waste heat recovery and thermal energy storage integration in air conditioning systems. *Energy Convers. Manag. X* **2024**, *24*, 100708. [CrossRef]

45. Zheng, Z.; Cao, J. Thermodynamic and feasibility analysis of air conditioning waste heat recovery via power generation cycles. *Energy Rep.* **2020**, *6*, 3472–3490. [CrossRef]